Spontaneous Assembly and Three‐Dimensional Stacking of Antiaromatic 5,15‐Dioxaporphyrin on HOPG

Chen, Tsang‐Wei Matt
Department of Chemistry and Center for Emerging Material and Advanced Devices National Taiwan University

Tanaka, Yuki
Department of Applied Chemistry Graduate School of Engineering, Kyushu University

Kametani, Yohei
Institute for Materials Chemistry and Engineering and Integrated Research Consortium on Chemical Science Kyushu University

Cheng, Kum‐Yi
Department of Chemistry and Center for Emerging Material and Advanced Devices National Taiwan University

他

出版情報：Angewandte Chemie International Edition. 61 (48), pp.e202212726-, 2022-10-26. Wiley
バージョン：

RESEARCH ARTICLE

Spontaneous Assembly and Three-Dimensional Stacking of Antiaromatic 5,15-Dioxaporphyrin on HOPG

Tsang-Wei Matt Chen[+],[a] Yuki Tanaka[+],[b] Yohei Kametani,[c] Kum-Yi Cheng,[a] Chih-Hsun Lin,[a] Yi Rick Lin,[a] Ting-Rong Hsu,[a] Zuqian Chen,[b] Jiping Hao,[b] Shigeki Mori,[d] Yoshihito Shiota,[c] Kazunari Yoshizawa,[c] Hiroyuki Furuta,[b] Soji Shimizu,*[b] and Chun-hsien Chen*[a]

[a] T.-W. M. Chen, K.-Y. Cheng, C.-H. Lin, Y. R. Lin, T.-R. Hsu, Prof. Dr. C.-h. Chen
Department of Chemistry and Center for Emerging Material and Advanced Devices,
National Taiwan University
Taipei 10617, Taiwan
E-mail: chhchen@ntu.edu.tw

[b] Y. Tanaka, Z. Chen, J. Hao, Prof. Dr. H. Furuta, Prof. Dr. S. Shimizu
Department of Applied Chemistry, Graduate School of Engineering and
Center for Molecular Systems (CMS), Kyushu University
Fukuoka 819-0395, Japan
E-mail: ssoji@cstf.kyushu-u.ac.jp

[c] Y. Kametani, Prof. Dr. Y. Shiota, Prof. Dr. K. Yoshizawa
Institute for Materials Chemistry and Engineering and
Integrated Research Consortium on Chemical Science, Kyushu University
Fukuoka 819-0395, Japan

[d] Dr. S. Mori
Advanced Research Center (ADRES), Ehime University
Matsuyama 790-8577, Japan

[+] These authors contributed equally to this work.

Supporting information for this article is given via a link at the end of the document.

Abstract: Antiaromatic compounds have recently received considerable attention because of novel properties such as narrow HOMO-LUMO gaps and facile formation of mutual stacking. Here, the spontaneous assembly of antiaromatic *meso*-2-thienyl-substituted 5,15-dioxaporphyrin (**DOP-1**) is scrutinized at the liquid-solid interface by scanning tunneling microscopy (STM). Polymorphism in monolayers characterized by the orthogonal and parallel assemblies is found at the low concentration of 0.05 mM. The parallel assembly is more stable and dominantly formed at higher concentrations. Aggregation was observed at concentrations > 0.2 mM, and the STM images of the aggregates implied the formation of stacked layers. The intrinsic electronic structures of the mutually stacked bilayer generated by applying an electric pulse to the monolayer were probed by scanning tunneling spectroscopy to reveal the narrowing HOMO-LUMO gap by ca. 20% from the monolayer, suggesting significant molecular orbital interactions.

Introduction

The term 'antiaromaticity' was introduced by Breslow in 1965 as an antonym of aromaticity to describe conjugated systems with 4nπ electrons when delocalization of the π electrons destabilizes the systems.[1] Although the definition of aromaticity/antiaromaticity is now classified in more detailed manners, such as Hückel aromaticity/antiaromaticity for planar and twisted molecules with 4n+2π/4nπ electrons,[2] Möbius aromaticity/antiaromaticity for 4nπ/4n+2π-conjugated molecules with a Möbius strip in the structures,[3–5] and Baird aromaticity for 4nπ/4n+2π-conjugated planar molecules in the excited state,[6,7] antiaromaticity in principle refers to unstable electron configurations.

In 2007, Schleyer *et al*. theoretically predicted that mutual stacking of two planar Hückel antiaromatic molecules within a distance for molecular orbital (MO) interactions can induce stabilized, degenerate HOMO, which resembles the electron configuration of aromatic molecules.[8] Such a through-space conjugated system was then described as a three-dimensional (3D) aromatic system. Despite the successful synthesis of antiaromatic compounds as a stable form in the last half-century,[9–12] molecular assemblies of antiaromatic molecules and their electronic structures have rarely been investigated because most stable antiaromatic molecules known to date possess bulky substituents to protect unstable antiaromatic conjugated systems in the core.

As stable, less sterically hindered antiaromatic molecules, a contracted porphyrin analogue called norcorrole[13] and heteroatom-substituted porphyrin analogues (heteroporphyrins)[14,15] were recently elucidated. Because of the removal of two sp^2-hybridized carbon atoms from the skeleton of porphyrin, norcorrole exhibits 16π antiaromaticity. In the case of heteroporphyrins, substitution of two sp^2-hybridized carbon atoms with amino-nitrogen atoms, oxygen atoms, or both generates structures of 5,15-diaminoporphyrin,[16,17] 5,15-dioxaporphyrin,[18] and 5-amino-15-oxaporphyrin[19] to attain 20π antiaromaticity. With the less sterically hindered antiaromatic porphyrin analogues in hand, Shinokubo *et al*. have investigated stacked structures of norcorrole. Their pioneering works revealed the reversal of the paratropic ring current effect to the diatropic one, indicating enhanced aromaticity.[20–22]

During our studies on single molecular properties of 20π antiaromatic Ni(II) 10,20-di(2-thienyl)-5,15-dioxaporphyrin (**DOP-1**, Figure 1) by scanning tunneling microscopy (STM), we noticed that **DOP-1** easily formed stacked assemblies at the liquid-solid interface on highly oriented pyrolytic graphite (HOPG). Motivated by the assembly formation for further study on the electronic

structure, the assembling processes of **DOP-1** were investigated by controlling sample concentrations. As a result, the monolayer formations were achieved at low concentrations, and the morphologies of assemblies were elucidated. Applying an electric pulse to the densely packed monolayer enabled the formation of the bilayer, the first example of stacked antiaromatic molecules observed at the liquid-solid interface. The scanning tunneling spectroscopy (STS) reveals the narrowing HOMO-LUMO gap of the stacked bilayer from the monolayer.

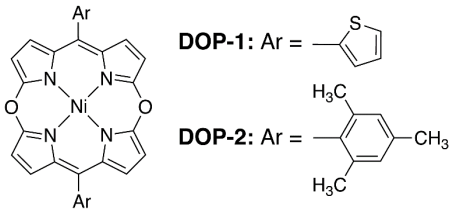

Figure 1. Structures of **DOP-1** and **DOP-2**.

Results and Discussion

DOP-1 was synthesized from Ni(II) bis(5-(2-thienyl)-1,9-dibromodipyrrin) under slightly modified reaction conditions from our previous study (See the Supporting Information).[18] The ^{1}H NMR spectrum of **DOP-1** exhibits slight downfield shifts of the β-pyrrolic proton signals at δ = 6.13 and 5.18 ppm from that of pyrrole at δ = 6.2 ppm due to the paratropic ring current effect arising from the 20π electron conjugated system (Figure S3). The weak paratropic ring current effect was supported by positive nucleus-independent chemical shifts (NICS(0))[23] values inside the macrocycle (Table S3). Single crystal X-ray diffraction analysis unambiguously elucidates two independent structures of **DOP-1** in the unit cell (Figures 2 and S4 and Tables S1 and S2).[24] Compared with the crystal structure of Ni(II) 10,20-dimesityl-5,15-dioxaporphyrin (**DOP-2**, Figure 1),[18a] **DOP-1** exhibits smaller dihedral angles between the *meso*-aryl substituents and the DOP core owing to the less steric hindrance of the 2-thienyl groups (**DOP-1**: 45, 57, and 79° and **DOP-2**: 81 and 89°). These small dihedral angles allow **DOP-1** to form a vertically stacked trimer with an interplanar distance of ca. 3.3 Å and Ni–Ni distance of 3.67 Å. The relative displacement of the nickel center by ca. 1.5 Å indicates a slipped stacking structure. Among the stacked three **DOP-1** molecules, the middle one exhibits a planar structure with a minor root-mean-square deviation (d_{rms}) of 0.02 Å, whereas the top and bottom ones are slightly deformed to take saddle-shaped structures with d_{rms} of 0.24 Å. Two **DOP-1** molecules in the stacked trimer each form complementary hydrogen bonding between the *meso*-oxygen atoms and the β-pyrrolic hydrogen atoms with a **DOP-1** molecule in the neighboring stacked trimer (Figure S4c,d). The harmonic oscillator model of aromaticity (HOMA)[25] values of these structures are 0.72 (planar structure) and 0.70 (deformed structures), indicating minor bond length alternations (Table S2). The NICS calculation was also performed on the stacked trimer. The positive NICS(0) values inside the macrocycles imply remnant antiaromaticity instead of 3D aromaticity (Table S4). This result can generalize the determinant factor of 3D aromaticity recently reported by Shinokubo *et al.* based on polymorphism of stacked norcorroles.[21b] They found that 3D aromaticity became distinct when two norcorrole molecules were stacked with a minor twist and a short displacement. In the current case, a poor overlap of the π-system due to the extensive displacement results in the absence of distinct 3D aromaticity.

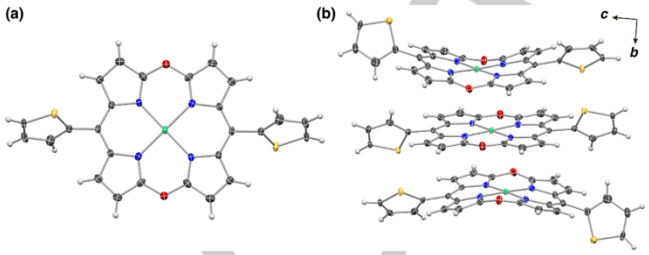

Figure 2. (a) X-Ray single crystal structure of **DOP-1**. One of the independent structures located in the middle of the stacked trimer is shown. (b) Stacked trimer in the packing diagram. The thermal ellipsoids are scaled to the 50% probability.

Figure 3 shows STM images of the **DOP-1** assembly at the liquid-solid interface of *n*-octanoic acid and HOPG at the sample concentration of ca. 0.05 mM. Figure 3a shows two motifs with staggered and striped features, encompassed by red and light-blue dashed lines, respectively. The underlying HOPG is exposed in the dark region, which can be a benchmark of the film thickness. The lower panel of Figure 3a is a cutaway view corresponding to the green horizontal line in the image. The height of ca. 2 Å for the assembly suggests that **DOP-1** molecules lie flat on HOPG. This model agrees well with reported values of 2–3 Å for porphyrin-based monolayers on HOPG and Au.[26,27] The staggered domains were rather unstable and transformed into striped domains within 30 min. Proposed adlayer models of the staggered domain and its morphological change to the striped domain are described in detail in the Supporting Information (section v and Figure S5).

Figure 3b shows polymorphs of the striped domain consisting of stripes with widths of 1, 2, and 4 **DOP-1** molecules. Among these morphologies in the striped domain, the dominant one is a dimeric stripe as shown in Figures 3c and S6a,e. The stripes are separated by dim channels. At the **DOP-1** concentration ≥ 0.2 mM, such dim channels do not develop, and the assembly appears to be densely packed (*vide infra*).

A high-resolution image of the striped domain is displayed in Figure 3c. Also presented is a proposed packing model derived from the lattice parameters as detailed in the figure caption, although possibilities of other types of arrangements are not ruled out. The assemblies are plausibly developed by the adsorbate-substrate attractions and intermolecular interactions, as indicated by the red circles. Two **DOP-1** molecules are arranged side-by-side in a parallel manner to form a rectangle-shaped dimer due to hydrogen bonding between the *meso* oxygen atoms and the β-pyrrolic hydrogen atoms. This building block is further organized into lengthy stripes by stacking the thienyl groups with the next neighbors. In the dim channels between the stripes, methylene chains of the co-adsorbed *n*-octanoic acid can be resolved. Co-adsorption of solvents with *n*-alkyl chains is frequently observed at liquid-solid interfaces[28–31] because of the van der Waals interactions with the HOPG substrate.[32] This dim channel formation is also facilitated by hydrogen bonding interactions

between the thienyl groups of **DOP-1** molecules and the acidic hydrogen atoms of co-adsorbed *n*-octanoic acid. The section profile (Figure S6e) shows that the dim channels are ca. 1 Å lower than the stripes, consistent with the relative difference in tunneling efficiency between the saturated alkyl chains and π-electron-rich moieties.

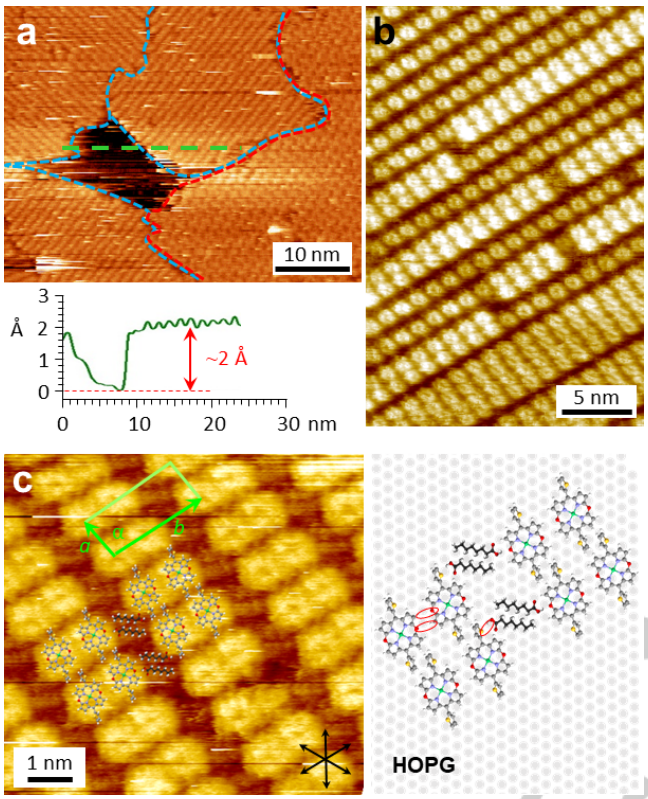

Figure 3. STM images of polymorphic **DOP-1** assembly. (a) The red and light-blue dashed lines indicate domain boundaries. The lower panel shows the section profile of the green dashed line in the middle of the image. (b) Stripes with widths of 1, 2, and 4 **DOP-1** molecules. (c) High-resolution STM images and proposed adlayer models of striped domains. The proposed intermolecular hydrogen bonds are circled in red. The arrows on the lower right of the image indicate the unit cell directions of the underneath HOPG. Unit cell parameters ($|\vec{a}|$, $|\vec{b}|$, α): 1.4 (±0.1) nm, 2.8 (±0.1) nm, 94 (±2)°. Image size: a) 38 nm × 58 nm, b) 30 nm × 20 nm, c) 8 nm × 8 nm. Conditions: **DOP-1** concentration, ca. 0.05 mM; solvent, *n*-octanoic acid; V_{bias} and $I_{tunneling}$, a) −1.0 V, 60 pA; b) −0.80 V, 60 pA; c) −0.80 V, 60 pA.

Upon increasing the **DOP-1** concentration to 0.2 mM, the STM images exhibit formation of large domains (> 200 nm × 200 nm, see also section viii in the Supporting Information). **DOP-1** molecules are closely packed in rectangle-shaped (Figure 4a,d) and parallelogram-shaped arrangements (Figure 4b,e). Figure 4c records the two structures in the same image to exclude the possibility of image distortion. The unit-cell structures are proposed in Figures 4d and 4e, and the lower panels manifest the difference arising from how the hydrogen bonds are paired. The rectangle-shaped arrangement is identical to the striped domain shown in Figure 3c without the dim channels. As for the parallelogram-shaped one, Figure 4f shows both the adsorbate and substrate in the same image to assign the overlayer structure to the underneath HOPG. At the lower part of the image, the tip V_{bias} was stepped down from −0.75 V to −0.020 V, an approach with a reduced tip-sample distance to unveil the underlying structure.[33] The 2D-FFT (fast Fourier transform) analysis revealed primitive unit cell vectors of 1.4 (±0.1) nm and 1.1 (±0.1) nm, approximately $\frac{10}{3}\sqrt{3}$ and $\frac{8}{3}\sqrt{3}$ times those of the underneath HOPG (Figure S7b,c). The unit-cell parameters are similar to those of the hydrogen-bonded packing structure observed in the crystal lattice of the single crystal (Figure S4c). These results indicate that the complementary intermolecular hydrogen bonding interactions (red dotted lines in Figure 4d,e) and π-π stacking of the thienyl groups facilitate the formation of the closely packed domains at high concentrations.

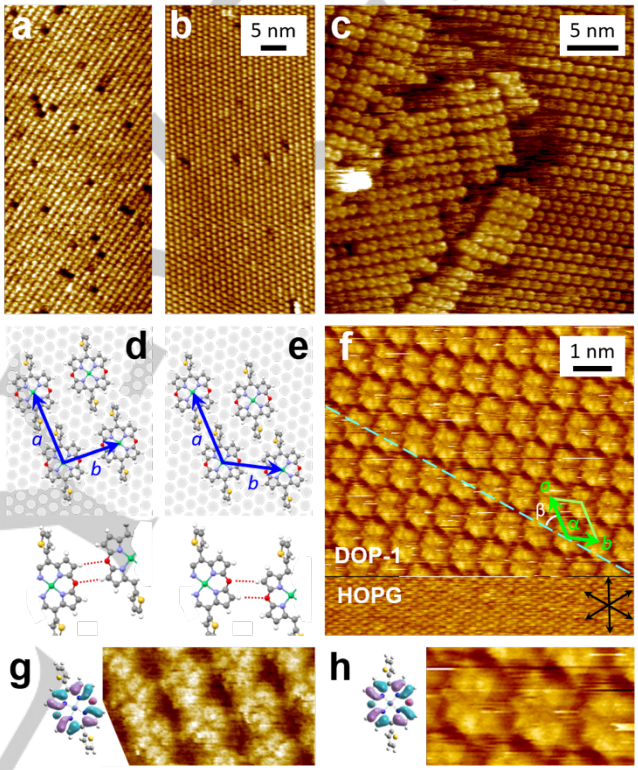

Figure 4. STM images and proposed models for the rectangle-shaped (a,d,g) and parallelogram-shaped (b,e,f,h) domains at the concentration of ca. 0.2 mM. Black arrows on the lower right of panel f indicate the unit cell directions of the underneath HOPG. One of the three directions, [1010], is in parallel to the dashed line across the center of the image to manifest the relative angles between the lattice vectors of adsorbate and substrate. In panels d and e, the red dotted lines indicate proposed intermolecular hydrogen bonds between the *meso* oxygen atoms and the β-pyrrolic hydrogen atoms. Image size: a,b) 29 nm × 60 nm, c) 30 nm × 30 nm, f) 8 nm × 8 nm. Unit cell parameters ($|\vec{a}|$, $|\vec{b}|$, α, β): rectangle-shaped domain, 1.4 (±0.1), 1.1 (±0.2) nm, 86 (±3)°, 30 (±3)°; parallelogram-shaped domain, 1.4 (±0.1) nm, 1.1 (±0.1) nm, 122 (±2)°, 30 (±2)°. Conditions: solvent, *n*-octanoic acid; V_{bias} and $I_{tunneling}$, a) −0.8 V, 45 pA; b) −0.8 V, 65 pA; c) −0.75 V, 50 pA; f, upper) −0.75 V, 40 pA; f, lower) −0.020 V, 60 pA; g) −1.2 V, 60 pA; h) −0.75 V, 40 pA.

The high-resolution images in Figures 4g,h show four-lobe features for the pyrrole groups of **DOP-1** under negative V_{bias} of −1.2 V and −0.75 V, respectively. The frontier orbitals calculated by the DFT method are displayed for comparison. The electron clouds of the HOMO resemble those of STM images, which exhibit a hollow at the molecular center due to the presence of a Ni^{2+} ion. Such features have been reported for the high-resolution STM images of Ni(II) porphyrins[34,35] and explained in terms of the electron tunneling mediated by the d_{z^2} orbital of the Ni^{2+} center.[36,37] Because the filled d_{z^2} orbital of the Ni^{2+} ion lies quite

far away from the Fermi level,[26,38–40] the contribution to the tunneling current is rather insignificant under the present imaging conditions, resulting in the hollow appearance at the molecular center. Unfortunately, the imaging quality at a more positive bias than +0.5 V was too deteriorated to find the LUMO signature. A possible reason may be the desorption of **DOP-1** molecules from the substrate due to unfavorable polarization under positive surface potentials[41–43] or competition of adsorption with *n*-octanoic acid solvent molecules.[41,44]

At **DOP-1** concentrations higher than 0.2 mM, it was difficult to obtain STM images due to aggregation and multilayer formation of **DOP-1** molecules. To mimic the initial growth of multilayered **DOP-1** assemblies and study the assemblies on monolayers, a high local concentration was created by applying a −4.5 V pulse for 10 μs to the closely packed monolayer at a concentration of 0.2 mM. Figure 5a shows that **DOP-1** molecules at the lower left part were ejected and readsorbed, resulting in small domains with flat terraces. The dark area in which **DOP-1** molecules were depleted shows features of HOPG. The section profile reveals a second layer of **DOP-1** molecules. The height of ca. 3 Å for the bilayer is less than twice as large as the monolayer thickness of 1.8 Å because the second layer imposes an additional attenuation in tunneling efficiency.[45,46] Further away from where the pulse was applied, **DOP-1** molecules were assembled to form lines along the direction of vector ***b*** (Figure 5b), the shorter one of the unit cell vectors (Figure 4d,e). The nodal planes of **DOP-1** molecules seen as faint dark lines imply the same orientations of the ground and second layers. To manifest such submolecular details, the bottom panels of Figure 5b are magnified from the green box in the middle panel. The contrast was significantly adjusted for the blurry fine lines at the ground (right panel, red arrows) and second layers (left panel, green arrows). Presently, we cannot completely rule out the possibility that the electric pulse might generate charged **DOP-1** species, which are dimerized with neutral **DOP-1** molecules on the ground layer. However, this mechanism is less possible because the densely-packed second layer formed with charged species might be unstable due to the electrostatic repulsion. The homogeneity of the ground and second layers in Figure 5b also support the formation of bilayer with neutral **DOP-1** molecules.

Applying a smaller pulse of −3.0 V for 10 μs can deposit a small amount of isolated **DOP-1** molecules (Figure 5c) without damaging the monolayer (Figure S9). It is discernible that the nodal planes (dark lines) for thus-deposited **DOP-1** molecules are generally in parallel with those of the ground layer. These images indicate that **DOP-1** molecules in the second layer are placed just above **DOP-1** molecules in the ground layer and form molecular chains by complementary hydrogen bonding interactions with the next neighbors and the π-π stacking of the thienyl groups as with the assemblies in the ground layer. Therefore, the observed stacking of two **DOP-1** molecules in the bilayer can be identified as a vertically stacked dimer of antiaromatic molecules.

STS (scanning tunneling spectroscopy) measurements were carried out to probe the intrinsic electronic properties of the **DOP-1** monolayer and bilayer. The *dI*/*dV* curve reveals the molecular density of states[47–49] and offers *in-situ* information about the vertically stacked antiaromatic molecules that cannot be obtained with other methods. Figure 5d displays *dI*/*dV* curves obtained at positions marked in Figure 5a. The spectrum of HOPG (black) is a reference curve and is relatively featureless within the bias window. In the spectrum of the **DOP-1** monolayer (red), the onset potentials around −0.50 V and 2.05 V defined by the intersections of the tangent at maximum slope and plateau line are assigned as the HOMO and LUMO energies of the **DOP-1** monolayer on HOPG, respectively (Figures S10 and S11, see section x in the Supporting Information).[50] The estimated HOMO-LUMO energy gap of ca. 2.55 eV is broadly reproduced by the DFT calculations on **DOP-1** molecule in the gas phase (2.20 eV (Figure S15)), whereas this value is smaller than that of 1.8 eV estimated from redox potentials in the cyclic voltammogram of **DOP-1** probably due to the polarization energy such as solvation energy that stabilizes the charged redox species in electrochemical environments (Figure S12).

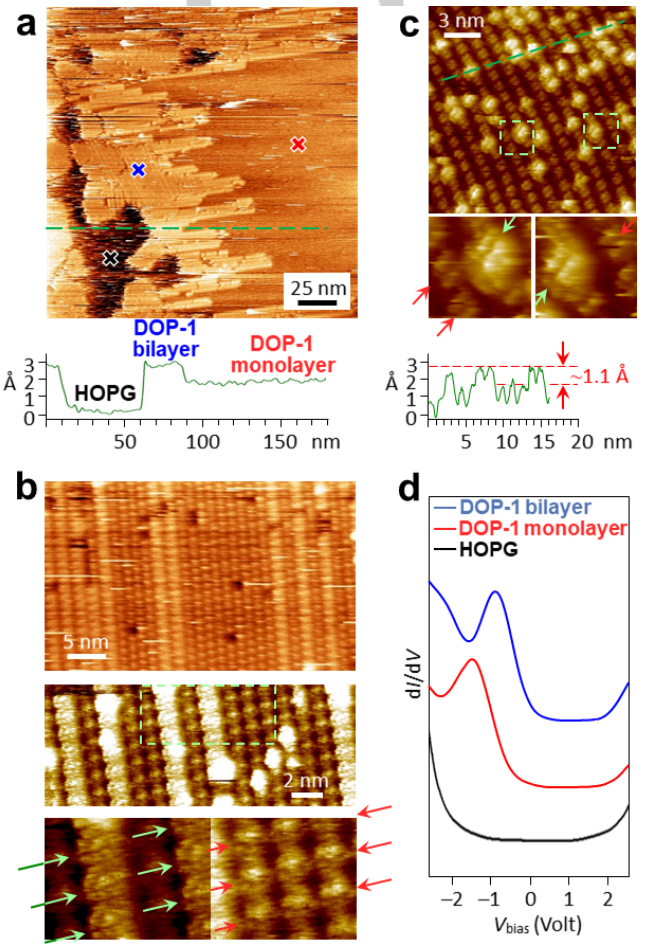

Figure 5. Topographic and STS analysis of the **DOP-1** monolayer and bilayer. (a) STM image of **DOP-1** assemblies after applying a −4.5 V electric pulse for 10 μs. Black, red, and blue cross represent positions of the STM tip, in which the *dI*/*dV* curves for the HOPG, **DOP-1** monolayer, and **DOP-1** bilayer were acquired in panel d, respectively. STM images of (b) molecular lines and (c) scattered **DOP-1** molecules deposited on the ground layer after a pulse of −4.5 V and −3.0 V, respectively. (d) *dI*/*dV* to the bias curves of the HOPG, **DOP-1** monolayer, and **DOP-1** bilayer. The HOMO band of the **DOP-1** bilayer around the bias potential of −1 V right shifts from that of the **DOP-1** monolayer. The height profiles acquired from the green dashed lines in panels a and c, showing the height difference between the **DOP-1** layers. The regions of green boxes in panels b and c are magnified in the lower panels. The red and green arrows indicate the faint dark lines of **DOP-1** monolayers at the ground layer and **DOP-1** molecular chains at the second layer, respectively. Image size: a, 200 nm × 200 nm; b (upper), 40 nm × 25 nm; b (middle), 20 nm × 7.8 nm; c, 17 nm × 17 nm. Imaging conditions (V_{bias}, $I_{tunneling}$): a, −0.8 V, 70 pA; b (upper), −0.75 V, 50 pA; b (middle), −0.75 V, 40 pA; c, −0.75 V, 80 pA.

The *dI*/*dV* curve of **DOP-1** bilayers reveals a narrowing of the HOMO-LUMO gap (2.01 eV) by ca. 0.5 eV compared with the monolayer. The HOMO onset shifts to the positive side. The trend qualitatively agrees with the spectral features of the Davydov splitting model for crystalline stacked organic films.[51–53] The DFT simulation with one **DOP-1** and two stacked **DOP-1** molecules on HOPG elucidates a shift of the HOMO toward the Fermi level, leading to a smaller HOMO-LUMO energy gap than that of the single molecule (Figures S13–S16, see section xii in the Supporting Information).[53–55] This result is inconsistent with Schleyer's prediction for so-called superphane-type model structures, in which two cyclic arenes with 4nπ-conjugation are linked to each other at each corner by a methylene (CH_2) unit.[8a] In his models, the MO interaction of degenerate singly-occupied MO (SOMO) of the antiaromatic cyclic arene and vertical stacking with small displacement are crucial for generating the stabilized, degenerate HOMO of the stacked superphane-type dimer. In the case of **DOP-1**, the D_{2h} molecular symmetry of the real molecule lifts the degenerate SOMO of the ideal 20π-electron cyclic annulene model of **DOP-1** to generate the non-degenerate HOMO and LUMO. In addition, there is a possibility that two **DOP-1** molecules can be stacked in a slipped stacking manner as observed in the crystal structure. Therefore, the antibonding and bonding MO interactions of the HOMO and LUMO, respectively, result in the Davydov splitting to cause the destabilized HOMO and stabilized LUMO. This discussion agrees well with the DFT simulation of the monomer and stacked dimer on the HOPG (Figure S16). Despite the discrepancy from Schleyer's prediction, narrowing the HOMO-LUMO gap of antiaromatic **DOP-1** by vertical stacking is beneficial for molecular electronics applications. This result also indicates that the strong tendency of antiaromatic molecules to form vertical stacking is not owed to the stabilized electron configuration but the intermolecular interactions, such as a dispersion force.

Conclusion

The STM studies on **DOP-1** at the liquid-solid interface reveal its spontaneous assembling processes to form monolayers at low concentrations ≤ 0.2 mM and layered assemblies at high concentrations > 0.2 mM. The morphologies of the monolayers largely depend on the concentrations; at low concentrations of ca. 0.05 mM, the phase transition was observed due to the interplay of the π-π stacking and intermolecular hydrogen bonding interactions between **DOP-1** molecules, solvent molecules, and graphite substrate, whereas at the concentration of ca. 0.2 mM, the densely packed structures similar to that in the crystal structure was obtained. The high-resolution image allows visualization of the HOMO. The facile formation of layered assemblies at high concentrations enables us to generate bilayers by applying a pulse of voltage to make a high local concentration. This is the first observation of the vertically stacked antiaromatic molecules by STM. The STS spectra reveal that the HOMO-LUMO gap of 2.55 eV for the monolayer becomes 2.01 eV for the bilayer. The reduced gap by ca. 0.5 eV is attributed to the Davydov splitting due to the antibonding and bonding interactions of the HOMO and LUMO of **DOP-1**, respectively. Although the electronic structure of the vertically stacked **DOP-1** is different from what Schleyer predicted for 3D aromaticity with the superphane-type model structures of stacked cyclic arenes,[8a] the current research gives two important insights; 1) stacking antiaromatic molecules in a slipped stacking manner can further decrease their inherently narrow HOMO-LUMO gaps that is a desirable feature for molecular electronics application, and 2) the strong tendency of antiaromatic molecules to form vertically stacked structures can be discussed from the viewpoint of energetic contribution rather than from that of electron configuration. The unique features of 3D aromaticity will be further investigated by the method developed in this study and reported in due course from our laboratories.

Acknowledgements

We thank Ms. Ting-Yin Liu for the preparation of STS spectra. The authors from National Taiwan University (NTU) are grateful to National Science and Technology Council (Taiwan, grant no. MOST 110-2123-M-002-004, 111-2123-M-002-008) and the Higher Education Sprout Project by the Ministry of Education (Taiwan) *via* NTU (grant no. 110L880515, 111L880515) for the financial support. The authors from Kyushu University thank the Japan Society for the Promotion of Science (JSPS) for the financial support (Grants-in-Aid for Scientific Research (B) (JSPS KAKENHI grant no. JP19H02703 and no. 22H02064)).

Keywords: antiaromaticity • heteroporphyrinoids • STM • STS

[1] R. Breslow, *Acc. Chem. Res.* **1973**, *6*, 393–398.
[2] a) E. Hückel, *Z. Phys.* **1931**, *70*, 204–286; b) E. Hückel, *Z. Phys.* **1932**, *76*, 628–648.
[3] E. Heilbronner, *Tetrahedron Lett.* **1964**, *5*, 1923–1928.
[4] H. S. Rzepa, *Chem. Rev.* **2005**, *105*, 3697–3715.
[5] R. Herges, *Chem. Rev.* **2006**, *106*, 4820–4842.
[6] N. C. Baird, *J. Am. Chem. Soc.* **1972**, *94*, 4941–4948.
[7] Y. M. Sung, M.-C. Yoon, J. M. Lim, H. Rath, K. Naoda, A. Osuka, D. Kim, *Nat. Chem.* **2015**, *7*, 418–422.
[8] a) C. Corminboeuf, P. v. R. Schleyer, P. Warner, *Org. Lett.* **2007**, *9*, 3263–3266; b) D. E. Bean, P. W. Fowler, *Org. Lett.* **2008**, *10*, 5573–5576.
[9] As representative studies on kinetically-stabilized antiaromatic compounds, see: a) A. Matsuura, K. Komatsu, *J. Am. Chem. Soc.* **2001**, *123*, 1768–1769; b) D. Hellwinkel, G. Reiff, *Angew. Chem. Int. Ed. Engl.* **1970**, *9*, 527–528; *Angew. Chem.* **1970**, *82*, 516.
[10] As a representative study on antiaromatic structures embedded into large aromatic structures, see: Y. Nakamura, N. Aratani, H. Shinokubo, A. Takagi, T. Kawai, T. Matsumoto, Z. S. Yoon, D. Y. Kim, T. K. Ahn, D. Kim, A. Muranaka, N. Kobayashi, A. Osuka, *J. Am. Chem. Soc.* **2006**, *128*, 4119–4127.
[11] As representative studies on antiaromatic compounds based on redox reactions of porphyrin and its analogs, see: a) E. Vogel, P. Röhrig, M. Sicken, B. Knipp, A. Herrmann, M. Pohl, H. Schmickler, J. Lex, *Angew. Chem. Int. Ed. Engl.* **1989**, *28*, 1651–1655; *Angew. Chem.* **1989**, *101*, 1683–1687; b) M. Pohl, H. Schmickler, J. Lex, E. Vogel, *Angew. Chem. Int. Ed. Engl.* **1991**, *30*, 1693–1697; *Angew. Chem.* **1991**, *103*, 1737–1741; c) B. K. Reddy, A. Basavarajappa, M. D. Ambhore, V. G. Anand, *Chem. Rev.* **2016**, *117*, 3420–3443; d) M. Kon-no, J. Mack, N. Kobayashi, M. Suenaga, K. Yoza, T. Shinmyozu, *Chem. Eur. J.* **2012**, 13361–13371; e) J. A. Cissell, T. P. Vaid, A. L. Rheingold, *J. Am. Chem. Soc.* **2005**, *127*, 12212–12213; f) J. A. Cissell, T. P. Vaid, G. P. A. Yap, *J. Am. Chem. Soc.* **2007**, *129*, 7841–7847.
[12] T. Tanaka, A. Osuka, *Chem. Rev.* **2017**, *117*, 2584–2640.
[13] T. Ito, Y. Hayashi, S. Shimizu, J.-Y. Shin, N. Kobayashi, H. Shinokubo, *Angew. Chem. Int. Ed.* **2012**, *51*, 8542–8545; *Angew. Chem.* **2012**, *124*, 8670–8673.
[14] Y. Matano, *Chem. Rev.* **2017**, *117*, 3138–3191.
[15] S. Shimizu, *Heterocycles* **2020**, *100*, 1123–1162.

[16] a) T. Satoh, M. Minoura, H. Nakano, K. Furukawa, Y. Matano, *Angew. Chem. Int. Ed.* **2016**, *55*, 2235–2238; *Angew. Chem.* **2016**, *128*, 2275–2278; b) K. Sudoh, T. Satoh, T. Amaya, K. Furukawa, M. Minoura, H. Nakano, Y. Matano, *Chem. Eur. J.* **2017**, *23*, 16364–16373.

[17] A. Yamaji, H. Tsurugi, Y. Miyake, K. Mashima, H. Shinokubo, *Chem. Eur. J.* **2016**, *22*, 3956–3961.

[18] a) A. Nishiyama, M. Fukuda, S. Mori, K. Furukawa, H. Fliegl, H. Furuta, S. Shimizu, *Angew. Chem. Int. Ed.* **2018**, *57*, 9728–9733; *Angew. Chem.* **2018**, *130*, 9876–9881; b) A. Nishiyama, Y. Tanaka, S. Mori, H. Furuta, S. Shimizu, *J. Porphyr. Phthalocyanines* **2020**, *24*, 355–361.

[19] K. Sudoh, K. Furukawa, H. Nakano, S. Shimizu, Y. Matano, *Heteroatom Chem.* **2018**, *8*, e21456–21411.

[20] R. Nozawa, H. Tanaka, W.-Y. Cha, Y. Hong, I. Hisaki, S. Shimizu, J.-Y. Shin, T. Kowalczyk, S. Irle, D. Kim, H. Shinokubo, *Nat. Commun.* **2016**, *7*, 13620.

[21] a) R. Nozawa, J. Kim, J. Oh, A. Lamping, Y. Wang, S. Shimizu, I. Hisaki, T. Kowalczyk, H. Fliegl, D. Kim, H. Shinokubo, *Nat. Commun.* **2019**, *10*, 3576; b) H. Kawashima, S. Ukai, R. Nozawa, N. Fukui, G. Fitzsimmons, T. Kowalczyk, H. Fliegl, H. Shinokubo, *J. Am. Chem. Soc.* **2021**, *143*, 10676–10685.

[22] S. Ukai, A. Takamatsu, M. Nobuoka, Y. Tsutsui, N. Fukui, S. Ogi, S. Seki, S. Yamaguchi, H. Shinokubo, *Angew. Chem. Int. Ed.* **2022**, *61*, e202114230; *Angew. Chem.* **2022**, *134*, e202114230.

[23] Z. Chen, C. S. Wannere, C. Corminboeuf, R. Puchta, P. v. R. Schleyer, *Chem. Rev.* **2005**, *105*, 3842−3888.

[24] Deposition Number 2132514 for **DOP-1** contains the supplementary crystallographic data for this paper. These data are provided free of charge by the joint Cambridge Crystallographic Data Centre and Fachinformationszentrum Karlsruhe Access Structures service www.ccdc.cam.ac.uk/structures.

[25] T. M. Krygowski, M. K. Cyranski, *Chem. Rev.* **2001**, *101*, 1385−1420.

[26] L. Scudiero, D. E. Barlow, U. Mazur, K. W. Hipps, *J. Am. Chem. Soc.* **2001**, *123*, 4073–4080.

[27] A. Ogunrinde, K. W. Hipps, L. Scudiero, *Langmuir* **2006**, *22*, 5697–5701.

[28] D. C. Y. Nguyen, L. Smykalla, T. N. H. Nguyen, M. Mehring, M. Hietschold, *Phys. Chem. Chem. Phys.* **2016**, *18*, 24219–24227.

[29] M. Ke, X. Tan, Y. Wang, B. Li, X. Zheng, X. Miao, X. Cheng, W. Deng, *J. Phys. Chem. C* **2021**, *125*, 19325–19332.

[30] M. Himmelhaus, F. Eisert, M. Buck, M. Grunze, *J. Phys. Chem. B* **2000**, *104*, 576–584.

[31] S.-L. Lee, Y.-C. Chu, H.-J. Wu, C.-h. Chen, *Langmuir* **2012**, *28*, 382–388.

[32] Fatima, M. Zepeda, N. Oncel, *Thin Solid Films* **2017**, *623*, 135–137.

[33] a) Q.-N. Zheng, X.-H. Liu, X.-R. Liu, T. Chen, H.-J. Yan, Y.-W. Zhong, D. Wang, L.-J. Wan, *Angew. Chem. Int. Ed.* **2014,** *53*, 13395–13399; *Angew. Chem.* **2014,** *126*, 13613–13617; b) J. D. Cojal González, M. Iyoda, J. P. Rabe, *Nat. Commun.* **2017,** *8*, 14717; c) O. Ochs, M. Hocke, S. Spitzer, W. M. Heckl, N. Martsinovich, M. Lackinger, *Chem. Mater.* **2020,** *32*, 5057–5065; d) Y. Fang, B. D. Lindner, I. Destoop, T. Tsuji, Z. Zhang, R. Z. Khaliullin, D. F. Perepichka, K. Tahara, S. De Feyter, Y. Tobe, *J. Am. Chem. Soc.* **2020,** *142*, 8662–8671; e) Y. Hao, G. Velpula, M. Kaltenegger, W. R. Bodlos, F. Vibert, K. S. Mali, S. De Feyter, R. Resel, Y. H. Geerts, S. Van Aert, D. Beljonne, R. Lazzaroni, *Chem. Mater.* **2022,** *34*, 2238–2248.

[34] T. Ohshiro, T. Ito, P. Buhlmann, Y. Umezawa, *Anal. Chem.* **2001**, *73*, 878–883.

[35] W. L. Deng, K. W. Hipps, *J. Phys. Chem. B* **2003**, *107*, 10736–10740.

[36] D. E. Barlow, L. Scudiero, K. W. Hipps, *Langmuir* **2004**, *20*, 4413–4421.

[37] A. Zhao, S. Tan, B. Li, B. Wang, J. Yang, J. G. Hou, *Phys. Chem. Chem. Phys.* **2013**, *15*, 12428–12441.

[38] X. Lu, K. W. Hipps, X. D. Wang, U. Mazur, *J. Am. Chem. Soc.* **1996**, *118*, 7197–7202.

[39] L. Scudiero, D. E. Barlow, K. W. Hipps, *J. Phys. Chem. B* **2000**, *104*, 11899–11905.

[40] F. Buchner, K. G. Warnick, T. Wolfle, A. Gorling, H. P. Steinruck, W. Hieringer, H. Marbach, *J. Phys. Chem. C* **2009**, *113*, 16450–16457.

[41] F. P. Cometto, K. Kern, M. Lingenfelder, *ACS Nano* **2015**, *9*, 5544–5550.

[42] S.-L. Lee, Y.-J. Hsu, H.-J. Wu, H.-A. Lin, H.-F. Hsu, C.-h. Chen, *Chem. Commun.* **2012**, *48*, 11748–11750.

[43] J. Ubink, M. Enache, M. Stöhr, *J. Chem. Phys.* **2018**, *148*, 174703.

[44] A. Mahmood, X. Zeng, A. S. Saleemi, K.-Y. Cheng, S.-L. Lee, *Chem. Commun.* **2020**, *56*, 8790–8793.

[45] Y. Kim, Y. Kim, J. Y. Park, *Langmuir* **2020**, *36*, 3792–3797.

[46] P. Samorí, A. Fechtenkötter, F. Jäckel, T. Böhme, K. Müllen, J. P. Rabe, *J. Am. Chem. Soc.* **2001**, *123*, 11462–11467.

[47] A. Selloni, P. Carnevali, E. Tosatti, C. D. Chen, *Phys. Rev. B* **1985**, *31*, 2602–2605.

[48] J. Tersoff, D. R. Hamann, *Phys. Rev. Lett.* **1983**, *50*, 1998–2001.

[49] R. M. Feenstra, W. A. Thompson, A. P. Fein, *Phys. Rev. Lett.* **1986**, *56*, 608–611.

[50] Q. Chen, T. Chen, G. B. Pan, H. J. Yan, W. Song, L. J. Wan, Z. T. Li, Z. H. Wang, B. Shang, L. F. Yuan, J. L. Yang, *Proc. Nat. Acad. Sci. U.S.A.* **2008**, *105*, 16849–16854.

[51] J. Cornil, D. Beljonne, J. P. Calbert, J. L. Brédas, *Adv. Mater.* **2001**, *13*, 1053–1067.

[52] D. Beljonne, J. Cornil, R. Silbey, P. Millie, J. L. Brédas, *J. Chem. Phys.* **2000**, *112*, 4749–4758.

[53] S.-L. Lee, M.-J. Huang, C.-h. Chen, C.-I Wang, R.-S. Liu, *Chem.–Asian J.* **2011**, *6*, 1181–1187.

[54] K.-Y. Cheng, C.-H. Lin, M.-C. Tzeng, A. Mahmood, M. Saeed, C.-h. Chen, *Chem. Commun.* **2018**, *54*, 8048–8051.

[55] S.-L. Lee, H.-J. Wu, Y.-J. Hsu, H.-H. Chen, H.-F. Hsu, C.-h. Chen, *Chem. Commun.* **2014**, *50*, 14093–14096.

Entry for the Table of Contents

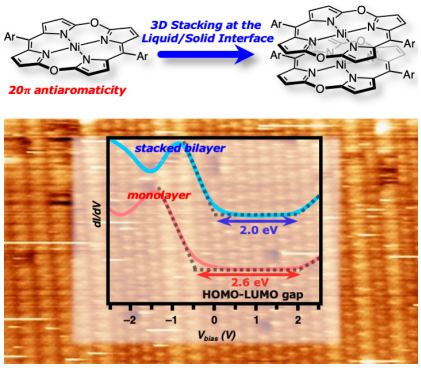

Spontaneous assemblies of antiaromatic *meso*-2-thienyl-substituted 5,15-dioxaporphyrin (**DOP-1**) have been studied at the liquid-solid interface to elucidate its polymorphism in monolayer and facile formation of the stacked layer. The study of the intrinsic electronic structures of the stacked bilayer by scanning tunneling spectroscopy revealed the narrowing HOMO-LUMO gap compared to the monolayer, thus suggesting significant molecular orbital interactions.

Institute and/or researcher Twitter usernames: ((optional))